Archaeological and Anthropological Sciences (2025) 17:60
https://doi.org/10.1007/s12520-025-02164-z

RESEARCH

Archaeology, chronology, and sedimentological context of the youngest Middle Palaeolithic assemblage from Jebel Faya, United Arab Emirates

Knut Bretzke[1,2] · Frank Preusser[3] · Kira Raith[4] · Gareth Preston[4] · Seolmin Kim[5,6] · Sabah Jasim[7] · Eisa Yousif[7] · Adrian G. Parker[4,8]

Received: 31 July 2024 / Accepted: 10 January 2025

Abstract
Due to the scarcity of stratified and well-dated archaeological horizons, diachronic as well as spatial patterns of Pleistocene lithic traditions are not very well understood in Arabia. To contribute to this topic, we present new archaeological, sedimentological and chronological data from archaeological horizon II (AH II), the stratigraphically youngest Middle Palaeolithic assemblage at Jebel Faya, Emirate of Sharjah, United Arab Emirates. Results of optically stimulated luminescence dating reveal that AH II was deposited about 80 ka ago at the end of Marine Isotope Stage 5 (MIS 5). The lithic assemblage shows a preference for elongated flakes and blades produced predominantly by bidirectional methods, both Levallois and non-Levallois. The few tools feature simple retouch often forming denticulated edges. Contemporaneous assemblages from Arabia are rare and show distinct technological characteristics, including a preference for the production of flakes with ovoid and triangular morphologies from centripetal as well as unidirectional convergent and bidirectional convergent Levallois methods. These differences indicate that traditions in the production of stone tool blanks follow distinct trajectories north and south of the Rub al-Khali desert at the termination of the MIS 5 humid period.

Keywords Arabia · Late Pleistocene · Palaeolithic · Lithic artifacts · Geochronology

Introduction

Palaeolithic records of Arabia are dominated by archaeological material that shows typical Middle Palaeolithic characteristics (e.g. Armitage et al. 2011; Rose et al. 2011; Delagnes et al. 2012; Petraglia et al. 2012; Crassard and Hilbert 2013; Jennings et al. 2016; Crassard et al. 2019; Groucutt et al. 2016, 2021; Bretzke et al. 2022). Among the most important Middle Palaeolithic traits found in Arabian assemblages are prepared core technologies including Levallois. Researchers distinguish different core reduction strategies, which produce different blank morphologies, including ovoid, triangular, and elongated flakes and blades. Based on the assumption that lithic reduction systems are linked to social learning processes, relative frequencies of distinct core reduction systems have been used to develop

✉ Knut Bretzke
knut.bretzke@uni-jena.de

1 Seminar for Prehistoric and Protohistoric Archaeology, University of Jena, Löbdergraben 24a, 07743 Jena, Germany

2 Department of Early Prehistory and Quaternary Ecology, University of Tübingen, Burgsteige 11, 72070 Tübingen, Germany

3 Institute of Earth and Environmental Sciences, University of Freiburg, Albertstr. 23B, 79104 Freiburg, Germany

4 Human Origins and Palaeoenvironments Research Group, School of Social Sciences, Oxford Brookes University, Gipsy Lane, Oxford OX3 0BP, UK

5 Institut d'art et d'archéologie, Université Paris 1 Panthéon-Sorbonne, 3 rue Michelet , Paris 75006, France

6 6-UMR 8068, Technologie et Ethnologie des Mondes PréhistoriqueS (TEMPS), MSH Mondes, Bâtiment René Ginouvès, 21 Allée de l'Université, 3 Rue Michelet, 92023 Nanterre Cedex, France

7 Sharjah Archaeology Authority, Government of Sharjah, Sharjah, United Arab Emirates

8 ARC Centre of Excellence for Australian Biodiversity and Heritage, University of Wollongong, Wollongong, Australia

Published online: 12 February 2025

hypotheses regarding the Pleistocene settlement history of Arabia (Rose 2010; Scerri et al. 2014; Groucutt et al. 2019; Bretzke and Herkert 2023).

Increased field work efforts over the past decade have revealed that archaeological records from Marine Isotope Stage (MIS 5; ca. 130–75 ka) are particularly common and were found in all parts of Arabia (Groucutt et al. 2021; Petraglia et al. 2012; Crassard et al. 2019; Rose et al. 2011; Armitage et al. 2011). However, as the number of meaningful sites (stratified and chronometrically dated) is still low, considering the size of the Arabian Peninsula, general conclusions regarding the occupation history are rather challenging. Nevertheless, it has been argued that sites in southern Arabia often feature assemblages with distinct local characteristics likely related to the presence of refugial areas in the South, while northern MIS 5 assemblages show more similarities with Levantine and Northern African technologies (Groucutt et al. 2021). Despite shortcomings of the Pleistocene archaeological records in Arabia, it has been further argued that Arabian MIS 5 assemblages commonly emphasise centripetal reduction systems, which is thought to reflect the spread of *Homo sapiens* in Arabia during MIS 5 (Blinkhorn et al. 2021). Due to the scarcity of well-dated archaeological material, however, diachronic, and spatial patterns of Pleistocene archaeological records and their potential causes are not well understood. Evidence clearly contradicting the conclusion of a dominance of centripetal Levallois in MIS 5 in southern Arabia, for example, is available from Dhofar, southern Oman. Here, substantial assemblages have been recovered that show a clear preference for bidirectional convergent Levallois systems producing triangular flakes (Rose et al. 2011). Chronometric data shows that this so-called Nubian technology occurs in southern Arabia latest at around 106 ka years ago (Rose et al. 2011).

The Palaeolithic site FAY-NE1 at Jebel Faya is situated in the central region of the Emirate of Sharjah, United Arab Emirates (UAE), approximately 60 km inland from both the Persian Gulf to the West and the Oman Sea to the East (Fig. 1). As one of the most complex Palaeolithic sites of Arabia, it covers the 20 m wide and 5 m deep Faya rock shelter as well as areas on the slope and on a terrace in front (Fig. 2). The rock shelter has developed into cretaceous limestone of the Buhais-Faya Mountain range. Excavations were conducted by joint projects between the University of Tübingen, Germany, and Sharjah Archaeology Authority from 2003 to 2017. Two main archaeological sequences have been described by the excavators. The first one was mainly recovered from the area in front of the rock shelter and includes, below an early Holocene layer dated to about 10 ka, a Palaeolithic sequence consisting of Assemblages A to D (Armitage et al. 2011; Uerpmann et al. 2013). Assemblage D was recently dated using optically stimulated luminescence (OSL) to about 210 ka and represents the oldest evidence for human presence at Faya (Bretzke et al. 2022). The stratigraphically younger Assemblages C and

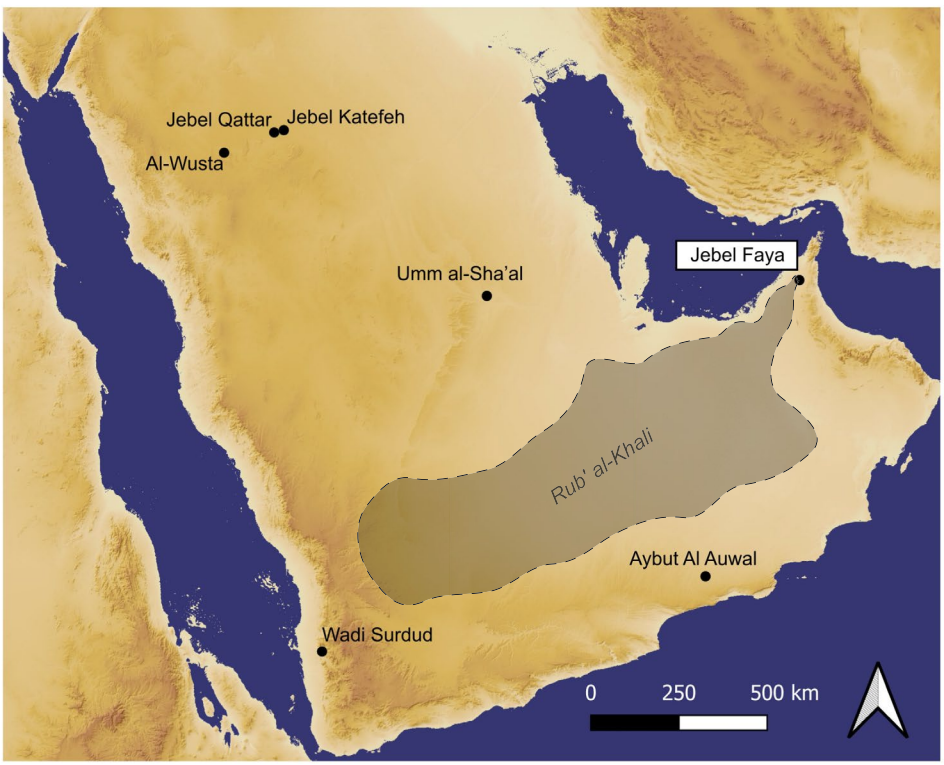

Fig. 1 Map showing the location of site FAY-NE1, Jebel Faya and other Middle Palaeolithic sites providing chronometric information mentioned in the text. Aybut Al Auwal (Rose et al. 2011), Wadi Surdud (Delagnes et al. 2012), Umm al-Sha'al (Crassard et al. 2019), Al-Wusta (Groucutt et al. 2018), Jebel Qattar & Jebel Katefeh (Petraglia et al. 2012)

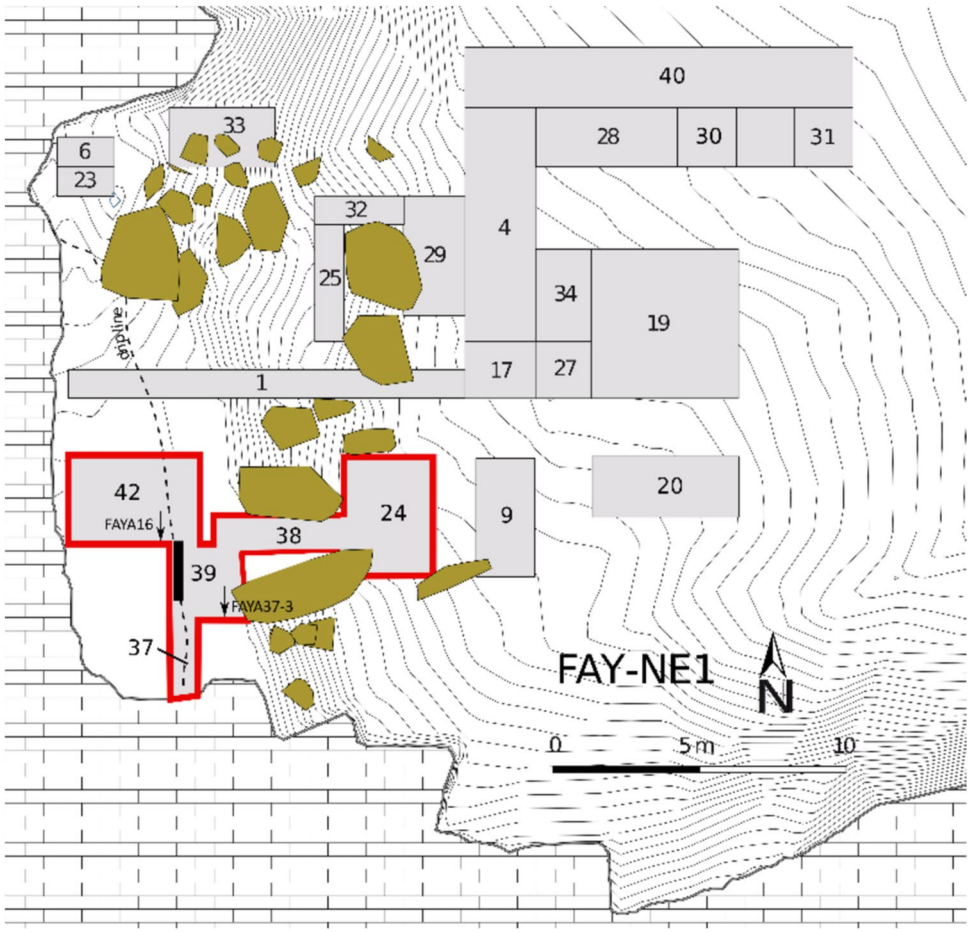

Fig. 2 Excavation plan. Excavated trenches, their locations and numbers are shown. Isolines in the background indicate topography. The red (bold) framed excavations trenches comprise the Faya Shelter sequence. The horizontal location of the OSL samples presented here are shown by the arrows in trench 42 and 37. Their vertical location is shown in Fig. 3. Please note the black bar in trench 39 shows the location of the profile shown in Fig. 3

A were OSL dated to about 125 ka and 40 ka, respectively (Armitage et al. 2011). No chronometric data is available for Assemblage B. The second sequence was excavated from the area beneath the modern rock shelter and extending to the transition area in front of it (Bretzke et al. 2014). This sequence comprises six palaeolithic layers (AH II-VII) and is named Faya Shelter sequence. The lowermost layer in the Faya Shelter sequence, AH VII, yields an age of about 170 ka, while AHs VI and V were dated to the time frame ca. 120–130 ka (Bretzke et al. 2022). The chronological range of the uppermost Palaeolithic layer of the Faya Shelter sequence, AH II, was previously determined by its stratigraphic position (Bretzke et al. 2014). Given that Bretzke et al. (2014) correlate AH IV of the Faya Shelter sequence stratigraphically with Assemblage A, it has been concluded that the overlaying AH II must be younger than 40 ka, likely postdating the Last Glacial Maximum, i.e., ca. 20 ka.

To expand the empirical foundation necessary for understanding the early prehistory of Arabia, we present new archaeological, sedimentological, and chronological data from the stratigraphically youngest Palaeolithic assemblage at site FAY-NE1. This includes an overview of typological and technological characteristics of the lithic artifacts found in AH II, comparisons with technological traditions from other regions, two new OSL ages, and analyses of sediment properties to characterize the environmental conditions during deposition. The present observations will be discussed in the context of available data regarding technological traditions and the environmental history of the Arabian Peninsula.

Material and methods

Excavation

About 240 m^2 have been excavated at Jebel Faya. The distribution of the archaeological layers is not uniform across the site since post-depositional developments such as flash floods and large-scale rock collapse have differentially affected the spatial preservation of the different occupation phases. We focus here on the archaeological assemblage of AH II, which is distributed exclusively under the modern rock shelter in trenches Tr 37, 39 and 42 of the Faya Shelter sequence (Fig. 2).

To excavate the archaeological deposits from the Faya Shelter sequence the site's established x–y-z coordinate system was extended into the southwestern part of the site. Excavations were carried out within defined trenches, using quarter meter units. Lithic artifacts larger than 2 cm, along with sediment from each bucket removed from the site, were piece plotted using a Leica Total Station. All excavated sediments were dry screened through 6-mm and 3-mm meshes. During the excavation at the Shelter sequence, the team identified archaeological (AH) and geological horizons (GH) based on sediment characteristics and the presence of archaeological material (Fig. 3). The horizon numbering increased from top to bottom. Sediment characteristics for each geological layer were documented and further analysed using sedimentological, micromorphological, and geochemical methods. The lithic assemblages were analysed following standard procedures, which included recording of morphological, technological, and typological characteristics.

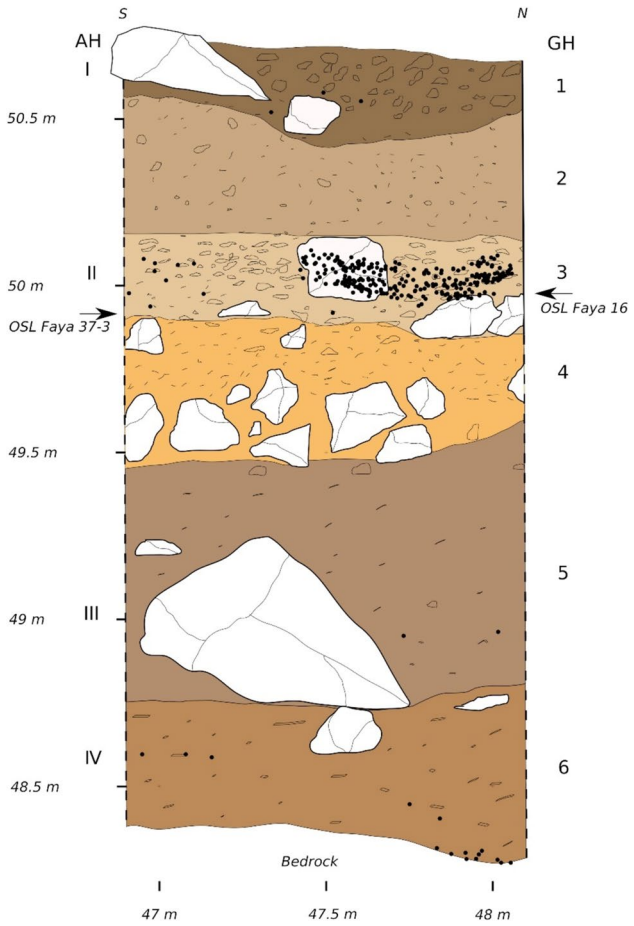

Fig. 3 Detailed sketch of the western stratigraphic profile of Trench 39, showing Faya Shelter sequence upper layers and vertical relation of AH II with OSL samples Faya 16 and 37–3. Please note that these OSL samples are located just north (Faya 16, Tr 42) and south (Faya 37–3, Tr 37) of this section (also see Fig. 2). GH = geological horizon, AH = archaeological horizon. Black circles indicate location of archaeological finds. Please note only those finds were plotted, which have been excavated 0–50 cm east to this profile

Luminescence dating

The often-cemented character of the Faya sequence sediments prevented the use of tubes for sampling the profile. Consequently, OSL sampling was carried out by collecting sediment samples through excavating sample locations at night using red headlights. It should be noted that the deposits investigated consist of relatively coarse material resulting from roof collapse, mixed with aeolian derived sand. To ensure sampling within and below the targeted layer, sampling locations have been carefully selected using x–y-z data from piece plotted artifacts of AH II. The sampling team first removed the outer, light-exposed layer and started collecting sediments after about 5–10 cm have been removed. The sediment extracted from the exposure was sieved on-site with a 2 mm mesh to significantly reduce the volume of material for shipping, which was transferred into opaque bags. A representative sample of about 200 g from the surroundings of each OSL sample was collected for high-resolution gamma spectrometry (non-sieved). This approach has the advantage of detecting radioactive disequilibria in the Uranium decay chain (e.g. Krbetschek et al. 1994; Olley et al. 1996; Preusser et al. 2023). Such disequilibria can arise in carbonate-rich sediments due to post-deposition mobilization from percolating water. Loss or gain of isotopes in the Uranium decay can lead to significant age offsets.

At the OSL dating lab of the University of Freiburg, the quartz fraction was extracted by sieving (100–150 µm), chemical treatments (10% HCl), density separation, and HF etching (cf. Bretzke et al. 2022 for further details). Equivalent dose (D_e) was determined using 1 mm aliquots (ca. 50 grains). Given that only around 3% of all grains from Jebel Faya exhibit strong luminescence emissions, i.e. a signal significantly above background (Armitage et al. 2011), the average number of grains per aliquot predominantly composing the detected signal is 1.35. Consequently, the small aliquot approach used here is very close to a single-grain level. All measurements were conducted using a Freiberg Instruments Smart device (Richter et al. 2015). The OSL decay curves are quite bright, dominated by the fast component, and show no issues with feldspar contamination (Fig. 4a). The single aliquot regenerative dose (SAR) protocol was employed (Murray and Wintle 2000), and preheating at 230 °C for 10 s was determined to be the appropriate procedure based on dose recovery tests (using the full SAR cycles used for D_e determination), with an average dose recovery ratio 1.03 ± 0.04, $n = 24$. Approximately 40 aliquots were measured per sample and fitted using a double-exponential saturating fitting curve (Fig. 4a, inset). A small number of measured SAR aliquots were rejected due to low signal

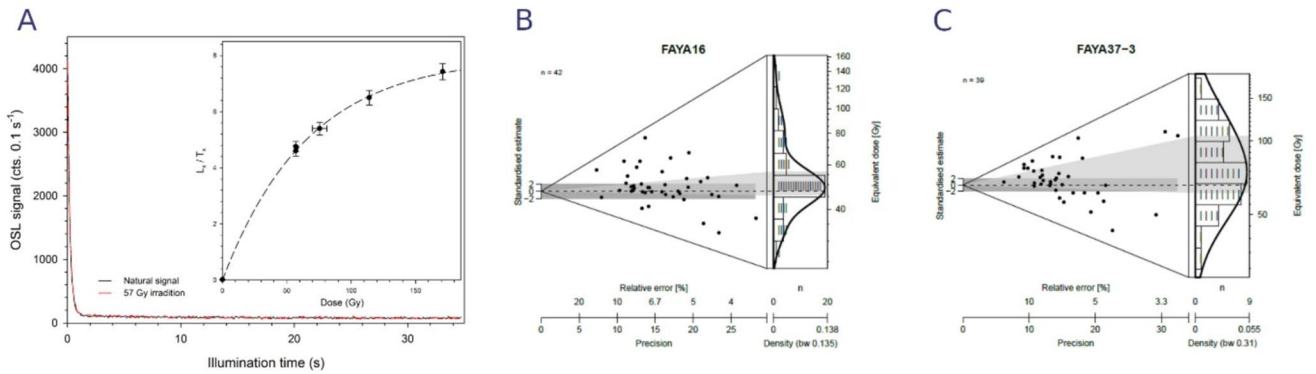

Fig. 4 **a** Most of the measured aliquots exhibit a rapid and uniform decay of both the natural and artificially irradiated OSL signals to a background level during optical stimulation. Inset: The growth of OSL signal with increasing given dose is best expressed by a double-exponential saturating function. Most aliquots are well below saturation limits. De distributions of samples FAYA16 (**b**) and FAYA37-3 (**c**) show tails towards both the lower and upper end. While for sample FAYA16 a dominant population of D_e values is clearly observed, it is less prominent in samples FAYA37-3

levels or failure to meet the rejection criteria of Wintle and Murray (2006). The total number of totally accepted aliquots is given in Table 1.

The D_e distributions for all samples are presented as Abanico plots (Fig. 4b, c; cf. Dietze et al. 2016). The average D_e values were calculated using the Central Age Model (CAM), the Minimum Age Model (MAM), and the Finite Mixture Model (FMM; cf. Galbraith and Roberts 2012). For the FMM, three components were assumed, and average values were computed using sigma_b values ranging between 0.15 and 0.25. The value showing the best fitting criteria (BIC) was selected for further analysis. The use of FMM is justified by the presence of three different processes contributing to the D_e distributions. The primary source is aeolian transport, which deposits well-bleached grains, as demonstrated by Bretzke et al. (2022) for modern analogues from the Faya site. A secondary source is the weathering of the rock shelter roof, as already discussed by Armitage et al. (2011). Although quartz content in the limestone is low, the volume of disintegrated roof material is considerable. Grains from this source may not have been zeroed at the time of deposition and could yield D_e values unrelated to sediment deposition age. Such D_e values should be excluded from average dose calculations. The third input could be post-depositional mixing, which introduces grains with an OSL signal indicating a daylight exposure time younger than the formation of the archaeological layer (cf. Armitage et al. 2011).

Material for dose rate gamma-spectrometry was dried, ground, and analysed at VKTA Rossendorf e.V. to determine the concentrations of K, Th and U (cf. Preusser et al. 2023). A comparison of the activities determined for U-238 and Ra-226 showed no evidence of radioactive disequilibrium in any of the samples. A water content of $3 \pm 3\%$ was assumed, reflecting the predominantly arid conditions of the region. Dose rates and ages were calculated using ADELEv2017 (Degering and Degering 2020; add-ideas.de), incorporating longitude, latitude and sample depth to account for the cosmic dose rate (Prescott and Hutton 1994). The dosimetric data and age results are summarized in Table 1.

The table also includes the, activity of the dose rate relevant elements (K, Th, U). For the latter, it presents the activity of the initial (U-238) and final part (Ra-226) to assess the potential for radioactive disequilibrium. D gives the total dose rate, n the number of aliquots measured/accepted for D_e determination, od. = observed overdispersion.

Sedimentological analyses

Sediment samples were systematically collected from open trench faces in TR42, TR37 and TR39 (Fig. 2). These were placed in zip lock bags. To determine organic carbon, carbonates, and inorganic sediment residue fractions, Loss-on-Ignition (LOI) was employed, following the method outlined by Heiri et al. (2001). Results were reported as percentages of dry weight. For particle size analysis, sediments were first dried in an oven at 105 °C for 12 h, then disaggregated using a rubber pestle and sieved through a 2 mm aperture sieve to remove clasts. The samples were then placed in beakers, dispersed in deionized water, and organics materials were removed by adding a few drops of 30% H_2O_2, followed by gentle heating on a warming plate until the reaction stopped. Excess peroxide was evaporated until dry. The samples were further disaggregated with deionised water and 10 ml of 5% sodium hexametaphosphate, and then agitated on an orbital mixer for 1 h. Grain size distribution was determined using a Malvern Mastersizer 2000 for the < 2 mm fraction. Sediment statistics, including mean, sorting, skewness, kurtosis were

Table 1 Summary of the OSL dating results, detailing the sample name, the assigned archaeological horizon, and the depth at which each sample was collected below the surface

Sample	AH	Depth (cm)	K (Bq/kg)	Th (Bq/kg)	U [U-238] (Bq/kg)	U [Ra-226] (Bq/kg)	D (Gy ka^{-1})	n	Od	CAM D_e (Gy)	Model D_e (Gy)	CAM Age (ka)	Model Age (ka)
FAYA16	II	75	74 ± 8	3.4 ± 0.3	7.4 ± 1.5	7.7 ± 0.6	0.59 ± 0.03	46/42	0.30	52.37 ± 2.51	47.14 ± 1.88	89 ± 6	**80 ± 5**
FAYA37-3	II	80	115 ± 12	4.8 ± 0.4	6.5 ± 1.4	8.8 ± 0.6	0.78 ± 0.06	40/39	0.34	75.19 ± 4.22	66.04 ± 3.72	96 ± 7	**84 ± 6**

calculated following the scheme proposed by Folk and Ward (1957). Geochemical analysis was performed using an Olympus Vanta pXRF.

Results

Excavations in trenches 37, 39 and 42 (Fig. 2), recovered about 50–60 cm below surface (Fig. 3) an assemblage of 1528 lithic artifacts (Table 2). These finds formed a well-developed horizon with a vertical distribution of about 25 cm. This layer and its artifacts were named AH II. About 15–20 cm below the main concentration, there is a stratigraphically separated scatter of lithic artifacts called AH IIa (n = 257). Given limited chronological resolution of OSL dating technique and similar typo-technological characteristics, AH II and AH IIa will be presented together. Layer AH II is overlain by AH I, a layer with mixed archaeological remains from several Holocene periods and an archaeologically sterile layer of about 50 cm thickness, which separates AH I and AH II.

Sediments associated with AH II were classified under GH 3, which is a 25 cm thick layer that is pale brown (Munsell Color chart: 10YR 8/3), well-cemented, and very dry (Fig. 3). The matrix of GH 3 is dominated by fine sand with some silt, while clasts are mainly of gravel size. The base of GH 3 is marked by a coarse fraction with pebbles ranging from 5–10 cm in size, creating a distinct boundary with the deeper geological layer GH 4.

Luminescence dating

To determine the age of the deposition of sediments containing AH II, samples were collected from GH 3 in trenches 37 and 42 (Fig. 2). The sampling locations, situated approximately 3 m apart horizontally, encompass both the top and bottom of AH II. Sample FAYA16 exhibits one distinct population at the lower edge of the distribution, which is well represented by both the MAM and the FMM. Due to the tail-like shape of the lower edge, we favour the FMM using a sigma_b of 0.20 ($D_e = 47.14 \pm 1.88$ Gy). The corresponding MAM D_e, however, is indistinguishable within errors (46.30 ± 3.63 Gy). For sample FAYA37-3, the tail towards lower values is much more prominent compared to FAYA16 and calls for the mandatory use of the FMM. The best BIC is observed for a sigma_b of 0.14 (76.363.95 Gy) and decreases to ca. 70 Gy when using higher values. Using the above FFM D_e values results in overlapping OSL ages of 80 ± 5 ka (FAYA16) and 84 ± 6 ka (FAYA37-3), which represents an average (CAM) estimate of the burial age of 82 ka ± 4 (Table 1).

Table 2 AH II. Parameter of excavation and assemblage overview

Lithic Artifacts	Volume	Area	Debitage	Cores	Tools	Artifacts/m^2	Artifacts/m^3
1528	2.4 m^3	20 m^2	1450	22	56	76	636

Sediment analysis

In the Faya rock shelter sequence, four primary sedimentary facies have been identified following the classification scheme of White (2007) and as previously outlined in Bretzke et al. (2022). These are as follows: Facies 1 (RD – rockfall deposits), which is further divided into two subtypes: RD1: Composed of clast-supported, unsorted, angular gravel to boulder-sized debris that is slightly weathered. These clasts originate from the Cretaceous Simsima Formation limestone, which forms the rock shelter's vault and represents breakdown deposits from block collapse (sensu White 2007). RD2: Consists of fine- to medium-grained sediment with a compositional affinity to the creamy yellowish-brown, fine-grained wackestone and/or lime mudstone of the host rock, resulting from its weathering. This process is observable on the exposed back wall of the rock shelter.

Facies 2 (FO – Fine-Grained Infiltrated Deposits) are characterized by fine-grained sediments that infiltrated the rock shelter. Facies 3 (AE – Aeolian Deposits) originate from external processes typical of the surrounding landscape. These sands have an orange hue due to a higher percentage of oxidized quartz grains. The sands to the west of Jebel Faya are composed of approximately 67% carbonate, 30% quartz, and 3% Fe–Mg-rich grains (Farrant et al. 2006). Facies 4 (WL – Water-Lain Deposits) consists of sediment reworked by water, including small gravel and debris similar in size to clasts from underlying and overlying beds, characterized by an open framework texture with an absent matrix (White 2007).

Sediment samples were collected from three trench sections (TR37, TR39, TR42) that traverse the AH II sequence(Fig. 2). It is important to note that there is some lateral variation in both the thickness of facies and size of clastic material (Fig. 5). TR42N is located closest the back wall of the current rock shelter and was collected from the northern profile wall of trench 42. The sequence here extends to a depth of 127 cm below the surface (50.83 m datum) and the base of the profile rests on bedrock (45.56 m datum). TR42S/39W is located further away from the back wall of the shelter and extends much deeper to 250 cm below the surface. Here the southern (TR42) and western (TR39) profile walls were sampled. Only the sequence from 48.30 m datum and above to the modern surface at 50.80 m datum are described here. Earlier occupation phases inside the rock shelter

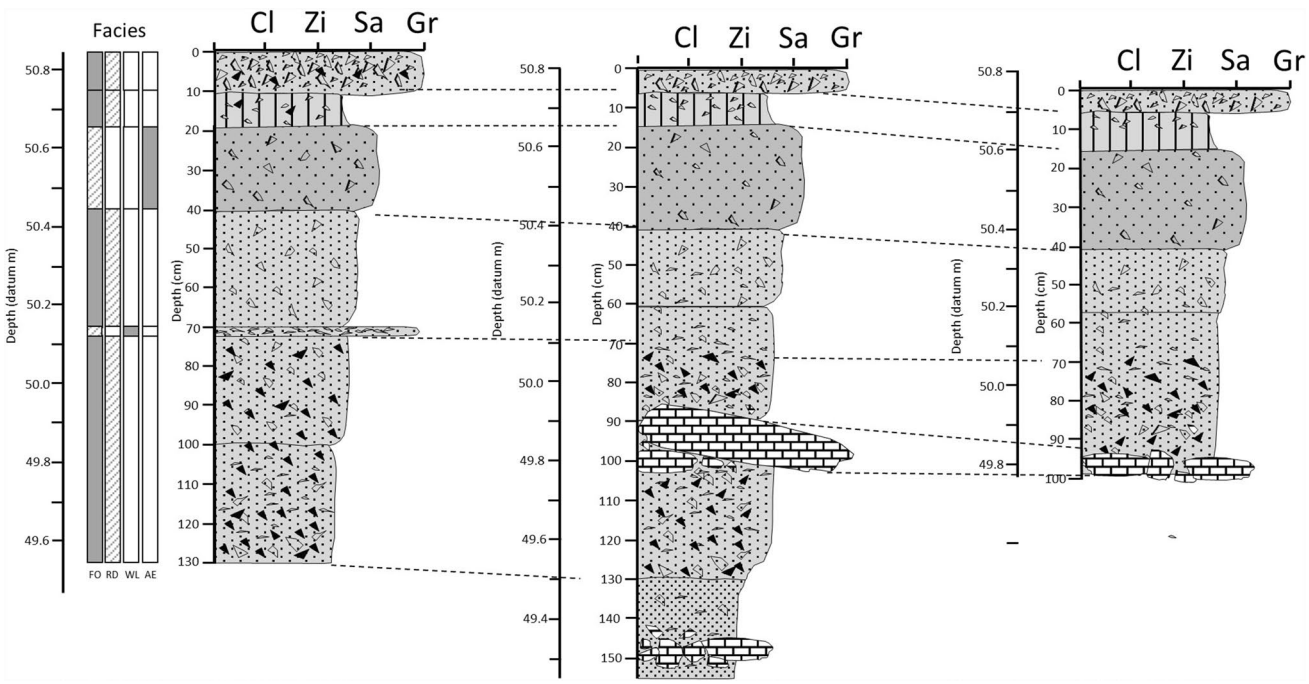

Fig. 5 Stratigraphic logs of the TR42N (left), TR42S/39W (middle) and TR37 (right) sediment profiles and correlations between these. Please note that we focus here on the upper parts of the profiles linked to AH II. Cl = clay, Zi = silt. Sa = sand, Gr = gravel

sequence, ranging from 210 to 120 ka, are reported in Bretzke et al. (2022). The sequence located outside of the rock shelter are reported in Armitage et al. (2011) and Bretzke et al. (2013). TR37 is located laterally to the east of TR42S/39W (Fig. 2). The sequence reported here is 100 cm deep (49.70 m to 50.70 m datum).

In TR42S/39W layer AH II is underlain by clast supported Facies RD1 rock fall material that is irregular owing to variations in clast size. This facies is located 152–142 cm below the surface (49.28 – 49.38 m datum) and comprises angular to sub-angular limestone clasts, which are up to 20 cm in length along the a-axis. The matrix (Facies FO) comprised weathered interstitial material which was visible between the rock fall clasts. Directly above the rock fall layer the sediment is matrix supported (Facies FO) with smaller limestone rock fall inclusions, which are weathered. The sediment comprises ~ 25% carbonates with silt and clay (up to 45%) and poorly sorted, coarse to very coarse skewed, leptokurtic, very fine sand (55%). The 60 cm thick AH II occupation layer starts at 130 below the surface (49.50 m datum) and continues until 70 cm below the surface (50.10 m datum). In this part of the sequence the AH II occupation layer can be divided into a lower layer AH IIa (49.50 – 49.75 m datum) and an upper layer AH II (49.95–50.10 m datum) separated by rock fall debris (Facies RD1) with no occupation material. Both AH IIa and AH II are characterized by Facies FO matrix supporting RD smaller clast inclusions (up to 5 cm) that become less concentrated and smaller in size (up to 2 cm) further up this unit. Facies FO comprised high carbonate values (~ 25%) with increased silt and clay contents (20–25%). The sediment is characterized by poorly sorted, coarse skewed, very leptokurtic, very fine to fine sand up to 160 µm in size. The Facies 1 (RD) rock fall deposit separating the AHII assemblage is characterized by carbonate values up to 28%, sand content (up to 85%) and low silt and clay content (up to 15%). The sediment is characterized by poorly sorted, near symmetrical, mesokurtic, fine sand up to 200 µm in size.

In TR37, layer AH II was found on top of the same upper rock fall (RD1 Facies) described in TR42S/39W, (which separated AH IIa from AH II). The AH II layer was located between 49.80 – 50.10 m OD (30 cm thick). In TR42N the AH II archaeological layer was 56 cm thick and rests on the limestone bedrock floor of the current rocks shelter (50.10 and 49.56 m datum). The AH I layer is not separated by rock fall material and is the equivalent to both AH IIa and AH II characterized only by a minor visual change in stratigraphy at 100 cm depth (49.85 m datum), which is the lateral equivalent to the rock fall layer observed in both TR42S/39W and TR37.

In all three sections (Figs. 6,7,8), above the archaeological horizon AH II, the sediments comprise matrix dominated Facies IO (to 40 cm below the surface in all three profiles), with fewer RD clast inclusions and an increasing AE aeolian component. The matrix becomes coarser in nature with an associated reduction in silt and clay content up profile. The sediments are characterized by fine skewed to near symmetrical, leptokurtic, fine sands (typically increasing from 90 to 130 µm in size). Up profile, carbonate content and Ca values decrease, while inorganic residue increases and magnetic susceptibility steadily rises. In TR42N, at a depth of 70 cm (50.12 m datum), a 2 cm thick, horizon dominated by clasts (WL Facies, indicating sediment sorted by water) is observed with fewer fines.

Between 40 cm and 20 to 15 cm depth in all three profiles (~ 50.40 to 50.65 m datum) the sediments mostly comprise sand sized material with the highest values reaching up to 86–88%. This unit is associated with matrix dominated Facies AE, which is mostly aeolian in nature with a minor RD component comprising small clasts up to 2 cm. The sediments are characterized by moderately sorted, near symmetrical, mesokurtic, fine sand up to 130 µm in size in TR37 and TR42S/39 and 200 µm in TR42N. Silt with no/negligible clay comprises up to 12% in this part of the sequence and carbonate values fall from 20 to 12%, with a corresponding increase in inorganic residue. The increasing

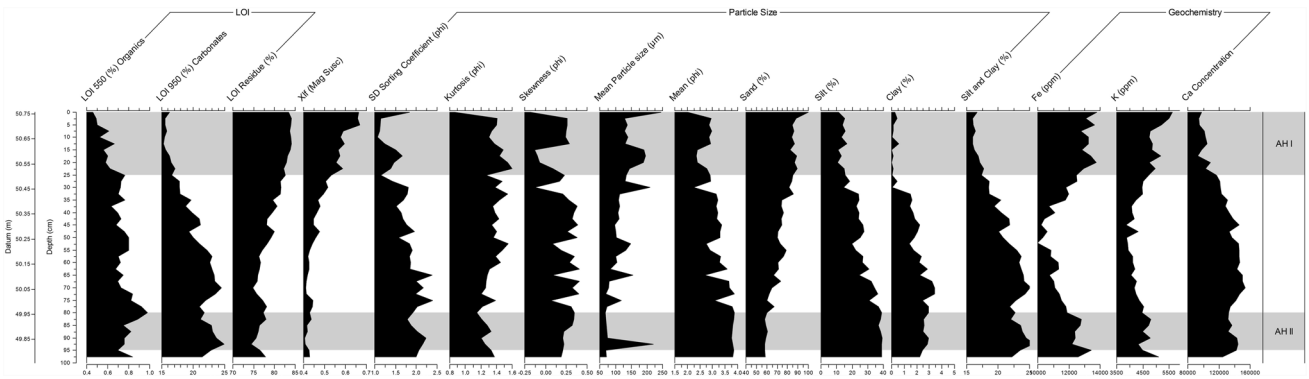

Fig. 6 Sedimentological diagrams for the TR37 profile showing zones and archaeological horizons (AH II and AH I)

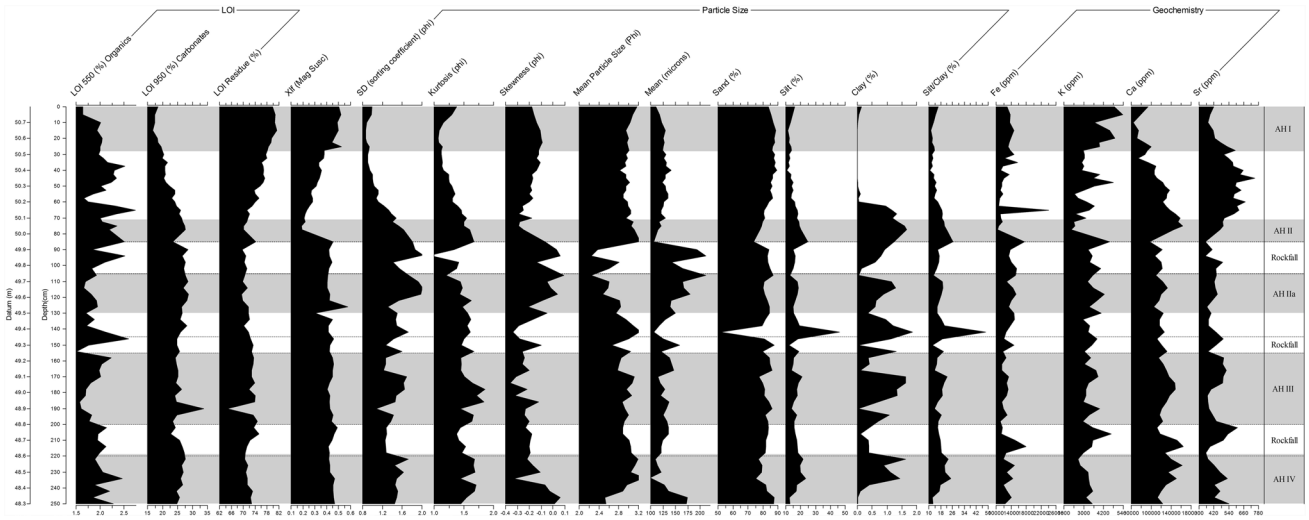

Fig. 7 Sedimentological diagrams for the TR42S/39W profile showing zones and archaeological horizons (AHs IV, III, II/AH IIa and AH I)

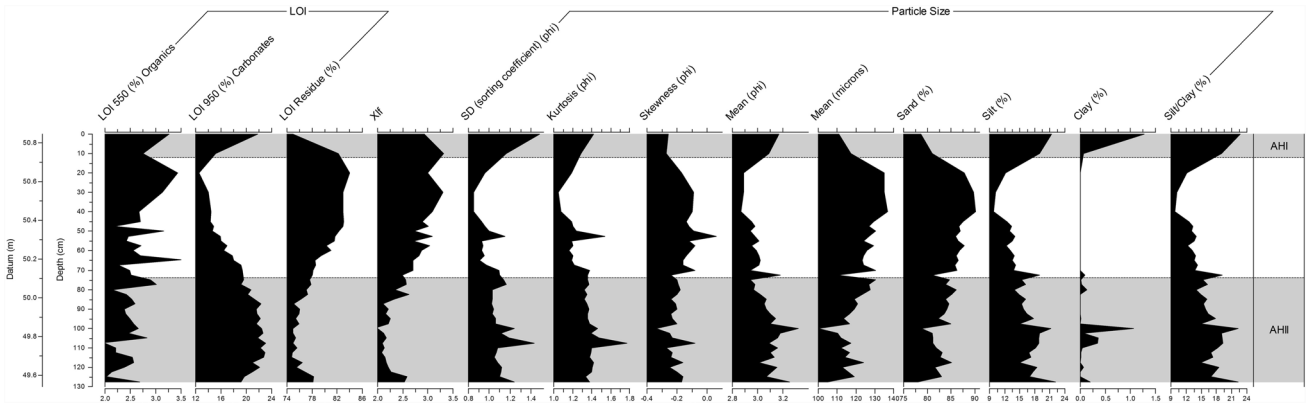

Fig. 8 Sedimentological diagrams for the TR42N profile

sand is associated with an increase in magnetic susceptibility values.

The uppermost parts of the three sequences comprise a finer grained unit (IO Facies with minor RD inclusions). These are capped by IO Facies, which form the land surface, comprising fine- to medium-grained sediment and an increased RD component derived from weathering of the rock shelter host rock. Carbonate values increase from 12 to 22%, increase in silts and clay and a reduction in the proportion of sand from 12 to 25% and decrease in sand from 88 to 68%. The sediment is characterized by poorly sorted, coarse skewed, leptokurtic very fine sand up to 110 µm in size. These upper units contain archaeological assemblage AH I.

The rock shelter sediments mostly comprise material derived from weathered limestone. Over time the breakdown of rock has led to recession and episodic collapse of the rock shelter overhang. Two phases of collapse are noted in the sequences described here. These are below AH II in TR37 and TR42S/39W and also between AH IIa and AH II in TR37. The collapsed layers comprise angular to subangular blocky limestone. The lower collapse layer pre-dates AH II so is older than 80 ka and the upper collapse layer occurred during the AH II occupation phase, separating the lower AH IIa from the upper AH II assemblage. Sediment composition of layers containing archaeological records is markedly different from those of archaeologically sterile layers, indicating occupation phases are linked to specific conditions (Fig. 9).

TR42N represents sediments that filled to current configuration of the rock shelter as the basal sediments which contain the AH II assemblage is located on bedrock. The AH IIa/AH II sediments mostly comprise finer-grained sediment with a higher silt and clay component derived from weathering and the breakdown of limestone rock fragments. This most likely occurred during phases of wetter climate conditions, which may have led to increased limestone dissolution

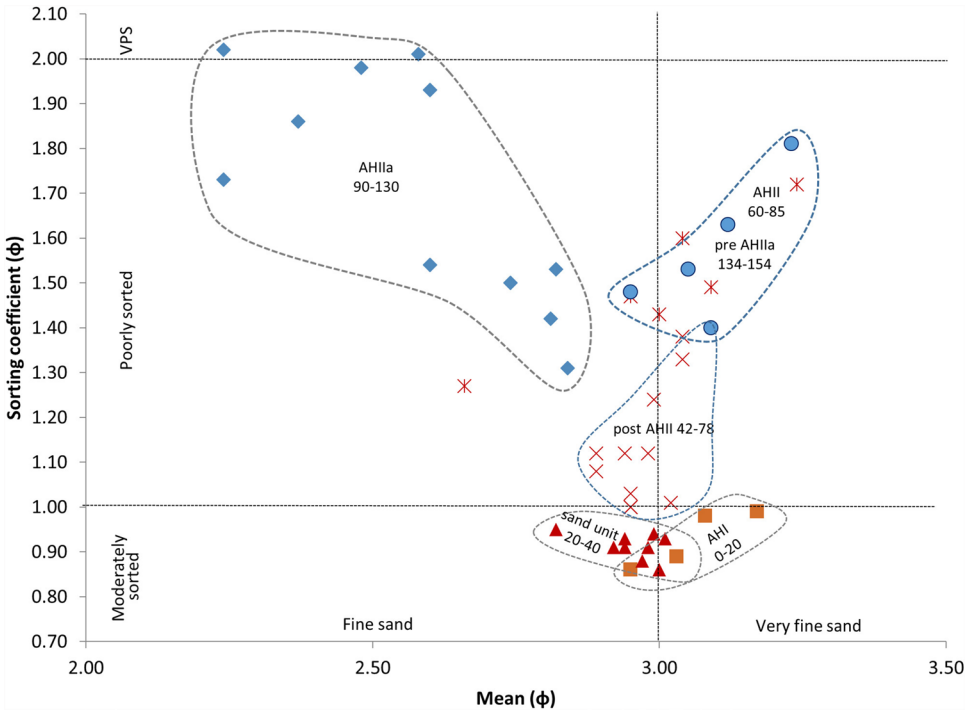

Fig. 9 Biplot of Mean (phi) vs Sorting Coefficient (phi) for sediments from TR42S/39W. Non-archaeological levels in red, occupation levels shown in blue

of the bedrock through the process of solution (Fookes and Hawkins 1988), but also increased mechanical weathering under wetter and warmer conditions (sensu Eppes and Keanini 2017; Eppes et al. 2020).

Archaeology

The archaeological record of AH II is exclusively composed of lithic artifacts (Tab. 2). Despite systematic dry screening and floatation of excavated sediments, we were not able to recover any organic material from AH II. Almost half of the recovered lithic artifacts are broken (see below). Apart from an increased proportion of fragmented artifacts, however, most lithics show well preserved and sharp edges and no secondary calcite crusts as regularly observed in the lithic assemblages of the deeper layers of the Jebel Faya sequence. Micromorphological, sedimentological and geochemistry analyses of the deposited sediments provide no evidence for significant post-depositional disturbances. We thus conclude that the composition and spatial distribution of the AH II assemblage were largely original and undisturbed.

Please note that the total number of lithic artifacts mentioned here includes only objects larger than 2 cm.

Lithic raw materials in AH II are dominated by brown and grey varieties of chert (> 90%), which occur locally in the Jebel Faya range (Fig. 10). Further variants include silicified serpentinite known to occur at a distance of about 15 km to the east, in the foothills of the al-Hajar Mountains. High quality, fine grained lithic raw materials of black and greenish varieties as well as examples showing a mixture

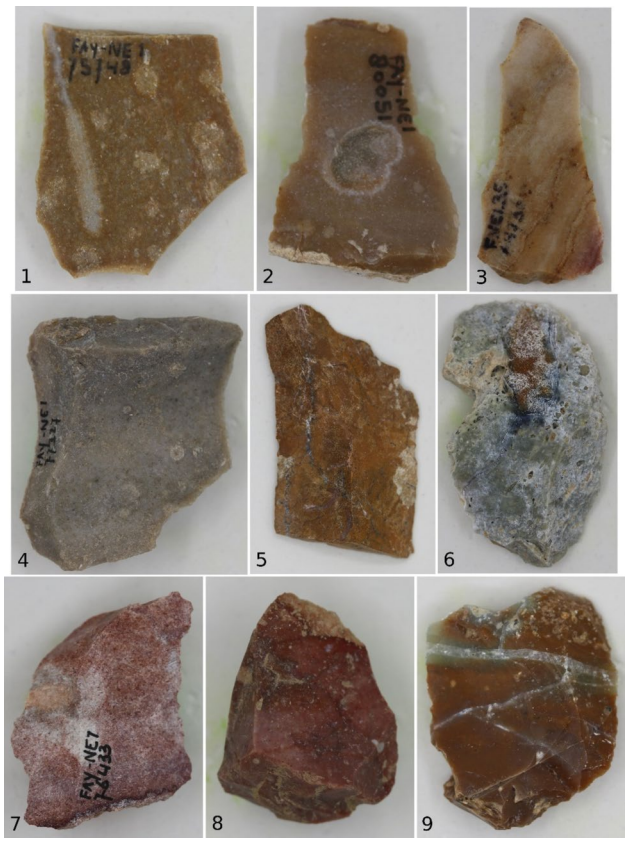

Fig. 10 Lithic raw materials. 1–3) brown chert varieties, 4) grey chert, 5 +9 silicified serpentinite, 6) greenish chert, 7–8) reddish chert variants. Known sources are located for 1–4 local (Jebel Faya), 5 + 9 about 15 km to the east, 6 about 30 km to the north. Potential sources for 7-8 are currently unknown

of colours ranging from grey to brown to black can also be found in small numbers (< 2%) in the AH II assemblage. They are known to occur in the Suhailah region about 30 km north of Jebel Faya. Reddish variants, including radiolarite, have also been observed in small numbers, but their localisation is currently unknown.

Cores of the lithic assemblage of AH II indicate an increased preference for bidirectional reduction systems (Table 3) compared to earlier layers in the sequence (please see Bretzke and Herkert 2023 for details). They are often relatively flat (mean thickness = 27 mm) and on average 51 mm long and 45 mm wide (Fig. 11). Thirteen cores feature two opposed platforms in the strict sense. On average, they are smaller than the other core type (L:50 mm, W:50 mm, T:24 mm). Two additional cores show two but offset and not strictly opposite platforms. Reduction surfaces of the bidirectional cores are mainly flat, but there are two examples with morphologies that can be classified as (sub-) cylindrical. Cores featuring a single striking platform with scars unidirectionally oriented (n = 1) as well as specimens with three and more striking platforms (n = 3) complement the core assemblage of AH II. These cores are shorter than the bi-directional cores and markedly thicker (L: 42 mm, W: 29 mm, T: 34 mm). Besides these nodule cores, there are three examples of cores on flakes. In these cases, thick flakes (mean = L: 66 mm, W: 52 mm, T: 25 mm) have been used to produce blanks from the ventral side with platforms installed in either one (n = 2) or two edges (n = 1). About 40% of the cores have prepared striking platforms as indicated through multiple scars (e.g. faceted). Reduction surfaces of about 30% of the AH II cores show scars with blade and elongated flake dimensions. This broadly agrees with the frequency of blades and elongated flakes observed in the AH II assemblage (25%, also see below). Reduction surfaces are mainly rectangular (n = 11) and ovoid (n = 5) in shape. Triangular shapes have not been observed in significant number in the AH II core assemblage.

One striking feature of AH II lithic assemblage is the presence of a laminar system. The entire knapping sequence, from decortication to obtaining of end-products, is present in the lithic assemblage and indicates that blade production was carried out on-site. Cores from the laminar system show minimal initial preparation and decortication. It is rather the selection of appropriately shaped raw material nodules with a natural crest at that intersection of two adjacent surfaces than the creation of a crest that allowed initiating the laminar production. The main striking platform on laminar cores was often installed on the wider face of the core. A second, opposed, striking platform was a frequently observed characteristics of the laminar cores. Preliminary results of the technological analysis indicate that opposed platforms were rather used to correct convexities and/or correct the guiding ridges than initiating a proper bidirectional reduction.

Besides blades, the AH II lithic assemblage clearly indicate a preference for elongated flakes. These flakes often show morphologies characterized by ogival distal ends and were produced by preferential and recurrent Levallois system using different methods of initialization (unidirectional convergent, bidirectional, multidirectional and centripetal) and production (unidirectional, bidirectional and centripetal). Levallois cores of the AH II assemblage (n = 2) have two faceted striking platforms, located opposed to each other.

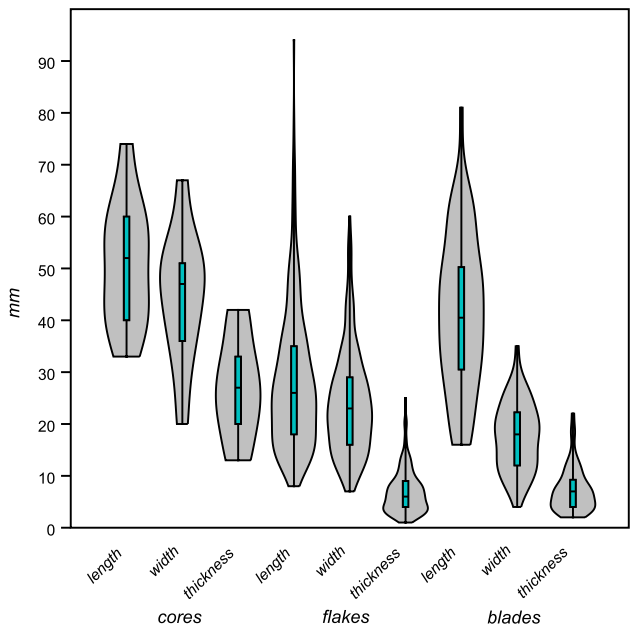

Fig. 11 Size ranges of complete cores, flakes and blades. Grey shaded area represents the frequency distribution of values shown as violine plot. Boxplots show median as horizontal line and the whisker's length represents one sigma

Table 3 Characteristics recorded on cores

Cores AH II	*n*
blank type	
nodule	19
flake	3
reduction type	
bi-directional	15
unidirectional	1
multiple platform	3
core on flake	3
platform preparation	
plain	13
faceted	9
scar types	
flake	16
blade	6

About 44% of the flakes and blades from AH II are fragmented. Among the complete artifacts are 313 flakes, 54 blades and 226 angular debris. Blanks with blade dimensions (twice as long as wide) form about 8% of the assemblage. When combing blades and elongated flakes (length to with ratio > 1.5, n = 95) this number rises to about one third of the blanks of AH II. While this estimate is in broad agreement with the scar frequency observed on the cores (see above), this number could still be a minimum estimate given that elongated morphologies break very easily and hence might be overrepresented in the category of broken artifacts.

Complete flakes from the AH II lithic assemblage are on average 28.3 mm long, 24.1 mm wide and have a maximum thickness of 6.9 mm (Fig. 11). The mean length to width ratio of complete flakes is 1.2. A closer look reveals that 95 out of 313 complete flakes (ca. 30%) have a length to width ratio of 1.5 and higher, indicating a that substantial part of the complete flakes can be classified as elongated. Regarding shape of flakes, the majority of flakes are rectangular and ovoid, while triangular morphologies form only a minority (Fig. 12). Dorsal scars on complete flakes show a dominance of the unidirectional and centripetal patterns. Bidirectional and unidirectional convergent patterns from together only 12%. Striking platforms of complete flakes are mainly plain, while about one quarter of the AH II complete flakes featured either faceted or dihedral platforms. Longitudinal profiles of flakes are mainly convex with about one third being straight (Fig. 13).

Blades of the AH II assemblage are on average 41.3 mm long, 17.6 mm wide and have a mean maximum thickness of 7.4 mm (Fig. 11). While blades average thickness is similar to those of flakes, the smaller width and larger length values indicate that blades have been intentionally produced and do not just form a by-product of the general reduction sequence. The mean length to width ratio is 2.5, which indicates rather compact blades. Plan shapes of the AH II blades are clearly dominated by rectangular morphologies (Fig. 12). Triangular shapes were identified on only 13% of the blades, which indicates that knapper did not focus on the production of pointed morphologies (Fig. 12). Dorsal scars on blades are mainly unidirectionally and bi-directionally oriented. Similar to the flakes, striking platforms on blades are mainly plain, with faceted and dihedral striking platforms forming together about one quarter. Blade profiles in AH II are equally frequent in convex and straight shapes. Twisted profiles occur slightly more often among blades than among flakes (Fig. 12).

The percentage of retouched artifacts is about 4% and hence relatively low (Table 2). The few tools are clearly dominated by rather simple retouch along lateral edges, while denticulated retouch variants do occur in addition (Fig. 14). If only part of the lateral edge has been worked, tools were classified as unsystematically retouched. This was the case in about one quarter of the tools. About half of the tools were made on elongated flakes and blades. Those flakes that have been used to produce tools come mainly (62%) from early stages of reduction (e.g. core preparation) featuring relatively increased cortex coverage. Regarding tool typology, most retouched lithic artifacts of the AH II assemblage can be classified as Middle Palaeolithic scraper, including types such as straight, transversal, and convergent sidescraper. Upper Palaeolithic types such as endscrapers on

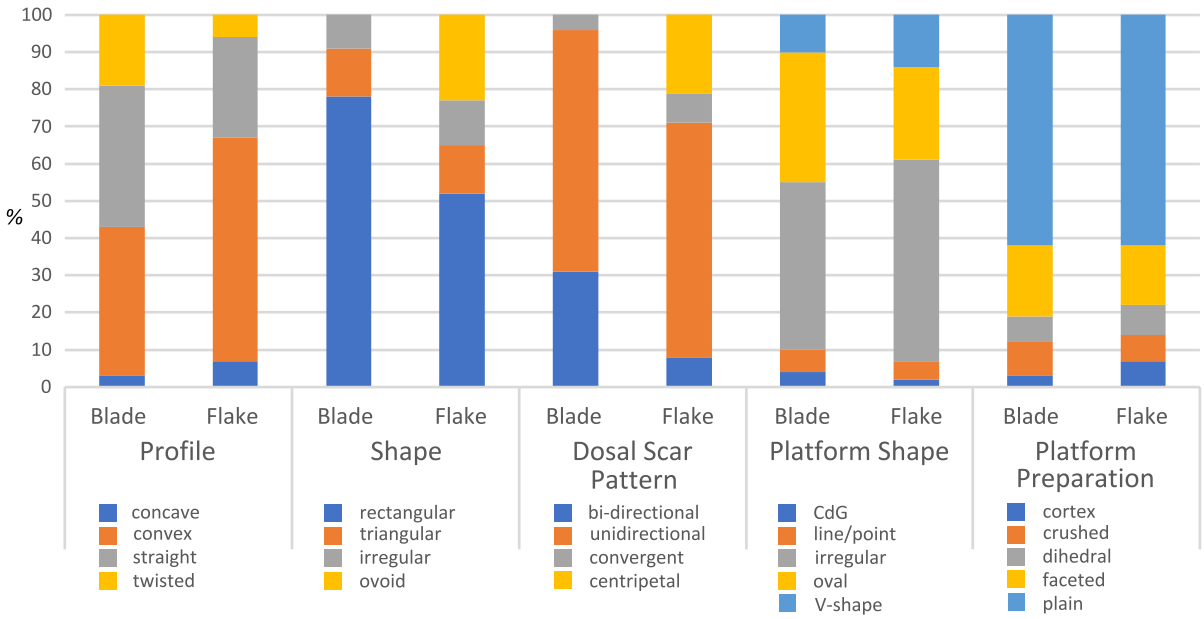

Fig. 12 Frequency of technological characteristics recorded on flakes and blades

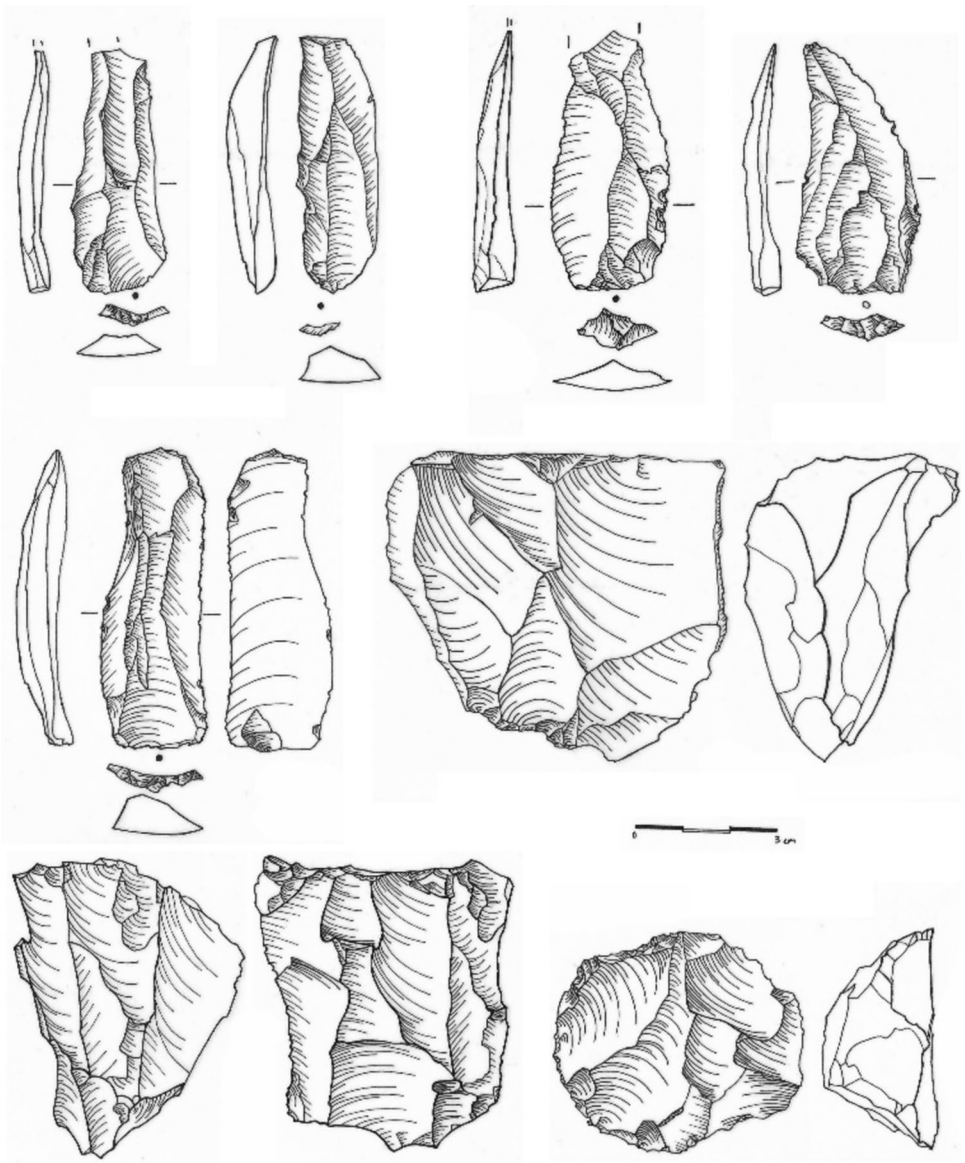

Fig. 13 Examples of components of the bi-directional reduction system

elongated blanks and one burin do also occur in the assemblage. The distinction between convergent scraper and point is not always straightforward. There are three specimens with convergent retouch that might be called point. While some lateral retouch occurs on the ventral side of the artifact, there is no evidence for bifacial retouch in the AH II assemblage.

In summary it can be said that the lithic assemblage from AH II shows a clear tendency towards the production of elongated artifacts using bidirectional reduction methods. There is no clear evidence for an intended production of pointed morphologies. The majority of elongated blanks features rectangular shapes with triangular variants representing a minority. The characteristic bidirectional reduction was observed on both, flat recurrent Levallois cores and (semi-) prismatic cores. Faceting of striking platforms was regular part of the technological repertoire of the group settling at Faya about 80 ka ago.

Discussion

The age estimation of the AH II deposits indicates that the youngest preserved Palaeolithic occupation at site FAY-NE1 took place about 80 ka ago during the final phase of MIS 5, considered to be a period with favourable climatic and paleoenvironmental conditions (Parker 2009; Atkinson et al. 2013; Drake et al. 2013). Subsequent occupation phases occur at Jebel Faya only after a significant chronological gap namely during the early Holocene about 10 ka ago (Armitage et al. 2011). Our results contradict previous conclusions about the possibility of a 40-ka occupation linked to AH IV

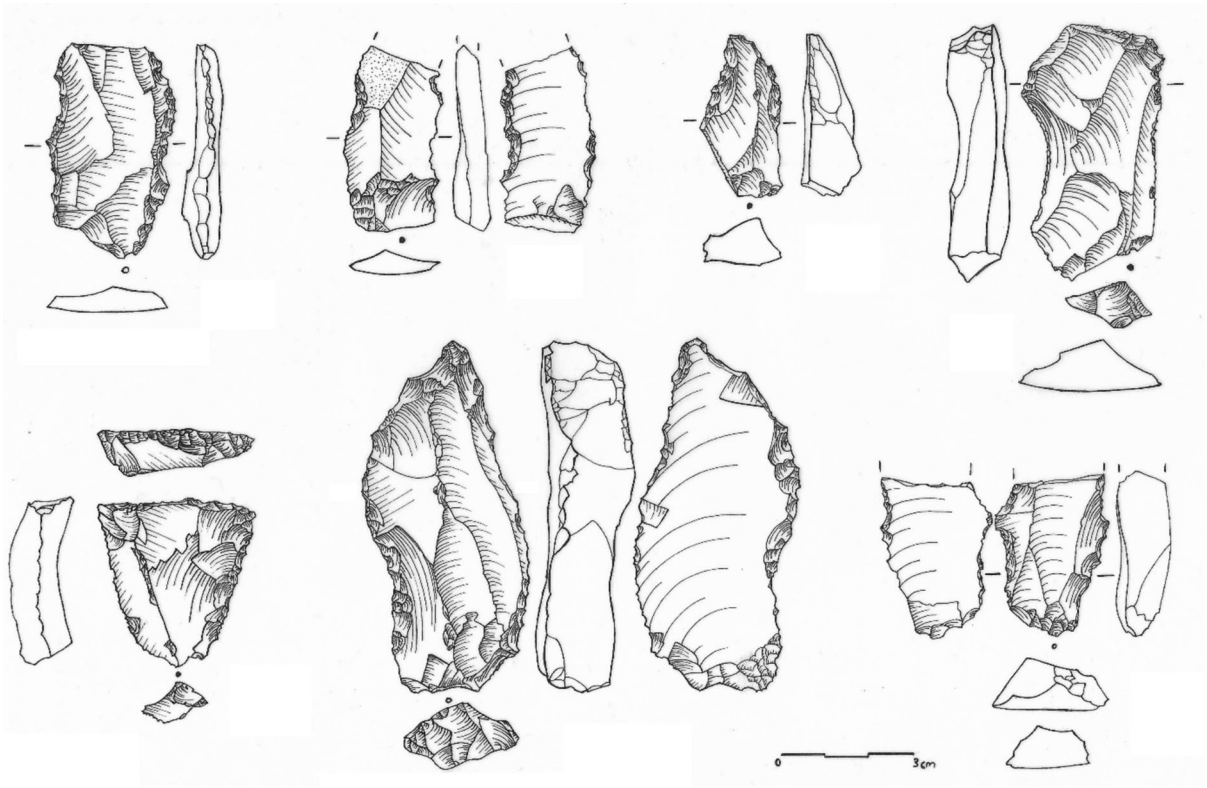

Fig. 14 Examples of retouched artifacts from AH II

(Bretzke et al. 2014). This conclusion was based on stratigraphic observations and a secure connection of AH IV from trench 38 with Assemblage A from the neighbouring trench 24 (Fig. 2). Assemblage A, however, has been dated to about 40 ka using OSL samples collected in the northern part of trench 4, at a distance of about 15 m from the Shelter sequence (Armitage et al. 2011). Given the complex colluvial character of sediments in front of the rock shelter, correlations over such distances are difficult. In contrast, the OSL sampling method applied here allowed controlled sampling of sediments directly associated with the AHs. We thus conclude that the Palaeolithic chronology for the Faya Shelter sequence, as presented here and elsewhere (Bretzke et al. 2022), includes exclusively occupation phases from the late early-Middle Palaeolithic and the mid-Middle Palaeolithic during MIS 6 and 5.

With the new results presented here, the Jebel Faya Shelter sequence demonstrates six occupation phases between ca. 170 ka and 80 ka. Bretzke and Herkert (2023) have published numerical data from lithic assemblages of the entire sequence. These data revealed a marked reduction of the flake volumes in AH II compared to artifacts from the earlier layers, while there is a general continuity in terms of basic lithic technology and typology throughout the sequence. However, their data also show a pronounced shift from centripetal Levallois and bifacial reduction systems for flakes in earlier MIS 5 (AHs VII-III) towards bidirectional reduction and a focus on the production of elongated flakes and blades at the end of MIS 5 (AH II). We side here with Bretzke and Herkert (2023) and argue that diachronic trends observed in the Faya Shelter sequence support the idea of shifting technological preference within the available repertoire during MIS 5. We do not see a significant change in the sense of an introduction of a developmentally unrelated technology.

Dated lithic assemblages from MIS 5a in Arabia are rare. Sites in the Nefud Desert in northern Saudi Arabia, including Jebel Katefeh, Jebel Qattar, and Al-Wusta (Petraglia et al. 2012; Groucutt et al. 2018) as well as sites from central Saudi Arabia such as Umm al-Sha'al (Crassard et al. 2019), provide evidence for humans in the interior of Arabia at approximately 80–90 ka. Archaeological assemblages excavated from the Nefud sites indicate lithic technological preferences distinct from those observed at Faya. In the Nefud, assemblages are characterized by flake production using centripetal Levallois and convergent methods (Scerri et al. 2014). At site Umm al-Sha'al, in central Saudi Arabia, there is a small bidirectional recurrent Levallois component in the upper assemblage, which, however, is associated with a certain convergent

component with Nubian affinities (Crassard et al. 2019). MIS 5a assemblages in Arabia, to the north of the Rub al-Khali desert, thus seem to indicate differences in the preferred way of producing stone tool blanks. Triangular and ovoid flakes are the goal of lithic production in central and northern Arabia rather than elongated flakes and blades as observed in the Southeast of the peninsula at Jebel Faya.

A widespread emphasis on centripetal Levallois reduction during MIS 5 has been proposed for both Arabia and the Levant (Blinkhorn et al. 2021; Prévost and Zaidner 2020). In the Levant, this characteristic has been used to differentiate between earlier and later Middle Palaeolithic entities (Shea 2013). Furthermore, the association of *Homo sapiens* fossils and lithic assemblages featuring centripetal Levallois methods in both the Levant (Hovers 1992) and Arabia (Groucutt et al. 2018), suggests a potential link between this reduction method and modern humans (Groucutt et al. 2015). In contrast, archaeological records from southern Arabia provide no clear evidence for a predominance of centripetal Levallois reduction in the later phases of MIS 5. The focus on the production of blades and elongated flakes using bidirectional reduction observed in Jebel Faya AH II at about 80 ka, is complemented by evidence from Dhofar, southern Oman, where significant records (e.g. from Aybut Al Auwal) show a focus on flaking systems geared towards the production of convergent morphologies often falling within the definition of the so-called Nubian technology (Usik et al. 2013). The occurrence of the latter in Dhofar has been dated to about 106 ka (Rose et al. 2011). It has further been argued that surface finds from Dhofar classified as Mudayyan, represent a development from classic Nubian technology into flat bidirectional reduction (Rose et al. 2019, p.57). The latter could have some affinities with Jebel Faya AH II and thus indicate a certain degree of connectivity between Dhofar and SE Arabia at the end of MIS 5. This, however, needs further detailed studies of the lithic material.

These examples indicate that there is likely no uniform, pan-Arabian developmental trajectory in terms of lithic material culture during MIS 5. In this context, the Rub' al-Khali could play an important role, separating traditions in the production of stone tools. Paleoenvironmental data, however, contrasts this conclusion, given that at least some parts of MIS 5 (substages e, c and a, for example) represent substantial wet periods in Arabia, some of which with evidence for permanent rivers, lake formations and potentially connected habitats. Hence from an ecological point of view it can be speculated that there were both, periods of connectivity and periods of isolation of different parts of the Arabian Peninsula during MIS 5. This reminds us, that climate and palaeoenvironmental change might not be the sole factors determining technological evolution in Arabia. What other determinants might be involved to explain distinct developmental trajectories north and south of the desert remains due to the scarcity of well-dated sites an exciting but currently open question.

The AH II phase of occupation at Jebel Faya falls within the global MIS 5a sub-stage (85–74 ka). According to Bretzke et al. (2022), linking global marine isotope records with regional climates is complex and confirming this connection with local records can be challenging due to often poorly constrained evidence and sometimes problematic age control. For Arabia, Bretzke et al. (2022) recommend using a regional climatic approach based on the Indian Ocean Monsoon (IOM) Index (Leuschner and Sirocko 2003). The IOM Index reflects precessionally-driven changes in monsoon intensity, based on latitudinal insolation differences (Clemens et al. 1991; Leuschner and Sirocko 2003), and it has been shown that increased precipitation in Arabia correlates with peaks in monsoon intensity (Parker 2009; Parton et al. 2015a, 2015b; Bretzke et al. 2022). This approach offers higher chronological resolution for parts of the Middle to Late Pleistocene compared to the approximately 100 ka eccentricity-driven periodicity used in glacial-interglacial models (Bretzke et al. 2022). Empirical evidence for human occupation in Arabia aligns well with odd-numbered Monsoon Index Peaks (MIPs) (Bretzke et al. 2022), which indicate increased monsoon intensity driven by higher insolation and greater seasonality across the Indian Ocean (Clemens et al. 1991). The AH II assemblage coincides with MIP 7 and the MIS 5a insolation peak (Fig. 15).

Palaeoenvironmental evidence in support of the MIP 7 peak comes from a number of regional sources (Fig. 16). Increased humidity in SE Arabia between 82–78 ka is recorded by rapid growth of both stalagmite and flowstone from Hoti Cave, Oman. $\delta^{18}O$ values during MIP 7 (MIS 5a) ranges between 6.5 and 4.0‰ and are similar to those recorded from the same site for the early Holocene but less depleted than for the last interglacial MIP 9 (MIS 5e, 130–120 ka) (Fleitmann et al. 2003). The northern Arabian Sea 93KL marine core record reveals depleted $\delta^{18}O$ values for the planktonic foraminifer *Globigerinoides ruber* between 85–74 ka (MIP 7/MIS 5a). This period is linked with an increased intensity of upwelling associated with the southwest monsoon (Schulz et al. 1998). This coincides with low detrital flux associated with reduced dust loading derived from terrestrial sources (Pourmand et al. 2004). This would infer a strengthened monsoon over the Arabian Sea and reduced aeolian input from Arabia due to wetter conditions at this time.

Within the Faya region, alluvial fan and fluvial wadi activation is recorded from a number of sites. Wadi Dhaid is an ephemeral stream with its headwaters located in the Hajar Mountains and a drainage basin in excess of 1,000 km^2. It runs, with its tributaries, over a distance of ~ 100 km and extends to the modern Arabian Gulf coast (Al Farraj and Harvey 2004). The catchment of Wadi Dhaid also drains part

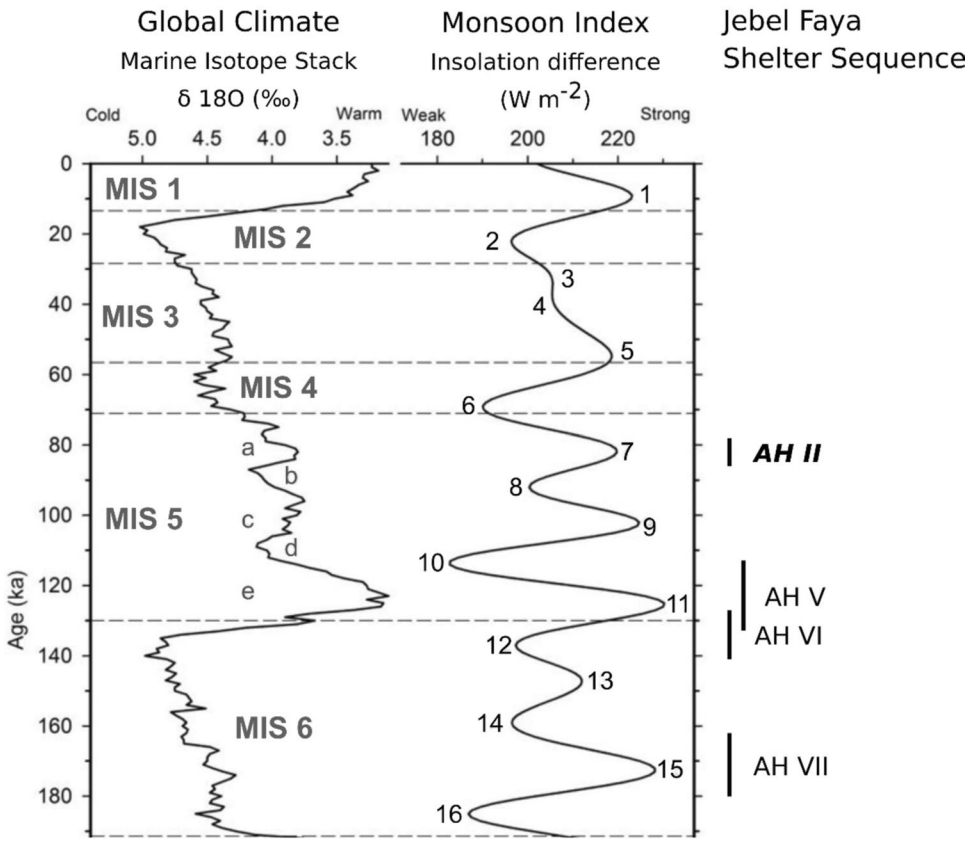

Fig. 15 Proxies for global climate development and dated archaeological layers from the Faya Shelter sequence. Shown age ranges represent calculated mean ages for AHs II, VI and VII and the result from one sample for AH V

of the Faya anticline including the northern and eastern part of Jebel Faya, which includes the FAY-NE1 archaeological site. At Tawi Asmar, located approximately 30 km downstream from Jebel Faya, in the medial to distal end of Wadi Dhaid, sand and gravel of the Hili Formation were dated between 110–76 ka (MIP 9 (MIS 5c) to MIP 7 (MIS 5a) (Atkinson et al. 2013). Approximately 90 km due south of Jebel Faya, proximal alluvial fan deposits and fluvial gravel of a relict palaeodrainage system have been dated between 85–74 ka (Atkinson et al. 2013; Farrant et al. 2012, 2015; Parton et al. 2015a, b). Perennial river flow created channels up to 20 m wide and at least 2 m deep, extending into the desert dune field of the Rub al-Khali (Atkinson et al. 2013). This fluvial evidence indicates increased wetness, the presence of perennial river channels, and widespread water availability across the regional landscape. Such conditions are crucial for standing early modern human presence in the region during MIP 7 (MIS 5a), as evidence by the AH II assemblage at Jebel Faya. Records from both Al Ain and Tawi Asmar reveal an extensive network of alluvial fans and fluvial channels that extended from the Hajar Mountains into the desert interior of the Rub' al-Khali and Arabian Gulf Basin (Atkinson et al. 2013; Farrant et al. 2012). These alluvial-fluvial networks would have been significant sources of water and provided viable routes for traversing the landscape during more favourable climatic conditions.

No additional age data are available from the three rock shelter sediment profiles in this study. However, it is worth noting that aeolian sand units outside the shelter at Jebel Faya have been previously dated to approximately 38.6 ± 3.2 ka (TR4) and 34.1 ± 2.8 ka (TR28) (Armitage et al. 2011), as well as 45.5 ± 3.9 ka and 44.6 ± 3.5 ka (TR36) (Russell 2014). Additionally, on the southern flank of Jebel Faya, an aeolian dune section (FDU) has been dated, showing 1.5 m of dune accumulation between 40.8 ± 3.2 and 37.0 ± 2.6 ka (Mueller et al. 2023). By association it is likely that the 20–25 cm thick sand unit found in TR42N, TR42S/39W and TR37 corresponds to the sand unit dated to ~ 40 ka (MIP 4) outside the shelter in TR4, TR28, TR26 and also the FDU section on the flank of the jebel. This suggests that increased aeolian sediment supply and dune deposition occurred at this time, which corresponds to MIP 4 (insolation minima). Further evidence for increased aeolian sediment flux comes from the northeastern Arabian Sea 93KL core record where there is a positive shift to less depleted $\delta^{18}O$ values for *G.ruber* ~ 40 ka (Schulz et al. 1998). From the same core an associated increase in mass accumulation rate (MAR) associated with increased aeolian dust flux was also noted (Pourmand et al. 2004). High dust fluxes to the northeastern Arabian Sea may be attributed to a weakened southwest monsoon with intensified northwesterlies from Arabia and Mesopotamia during MIP 4.

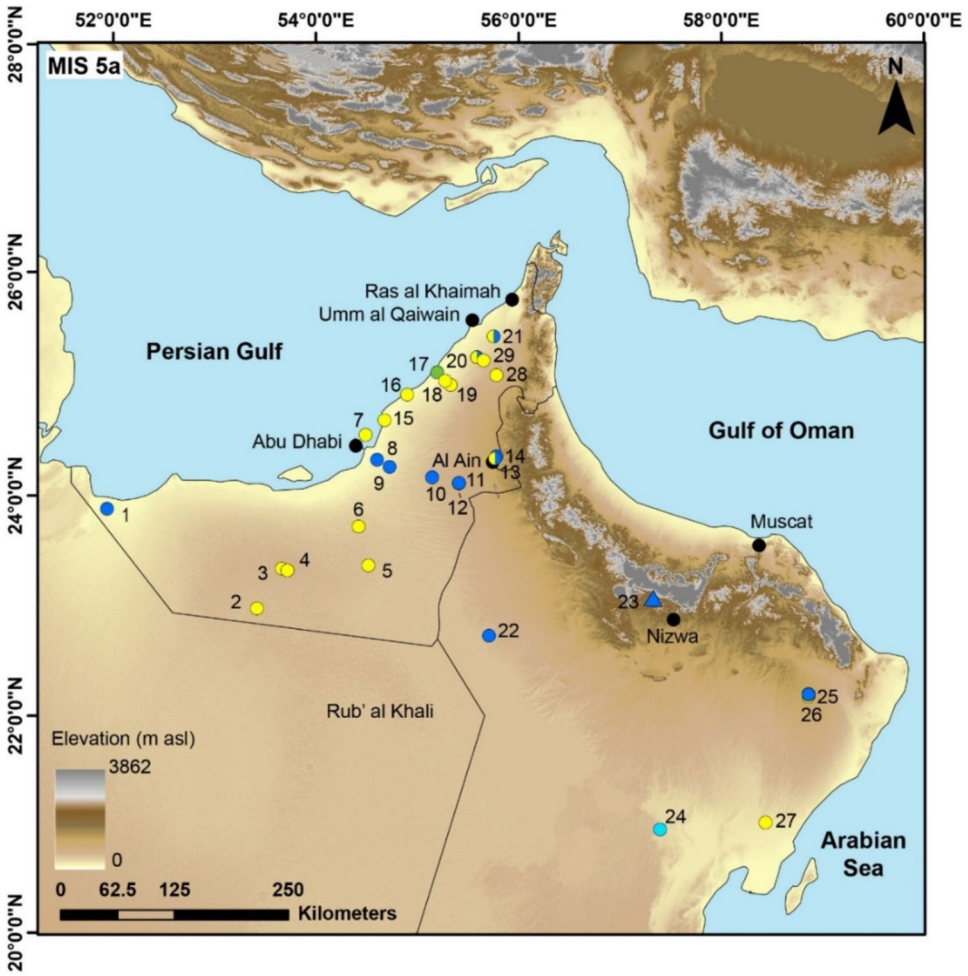

Fig. 16 Palaeoenvironmental records of MIS 5 on a digital elevation model (ALOS) of Southeast Arabia with fluvial (blue circle), lacustrine (light blue circle), speleothem (blue triangle), aeolian (yellow circle) and coastal (green circle) sites: ARF_2381 (1), Liwa 47 (2), AFIN_509 (3), Liwa pit/9–17 (4), ARF_1490 (5), Liwa AD-3B (6), ARF_2901 (7), ARF_1635 (8), ARF_1800 (9), BTHOMAS_152 (10), RAS_178 (11), ARF_2892 (12), Al Sibetah (13), Al-Ain (14), ARF_2878 (15), ARF_2879 (16), DUB 6 (17), SPRICE_31 (18), SPRICE_154 (19), ARF_2884 (20), Tawi Asmar UAE 06–3 (21), OM2 (22), Hoti (23), Saiwan (24), WDR 1 (25), WID & WIL (26), AJS (27), AQP (28), IDD (29)

Located on the upper contact of the Jebel Faya aeolian dune sediment in TR4, Faya points (lithic projectile points) have been dated to the early Holocene, around 10.5 ka (Armitage et al. 2011; Uerpmann et al. 2013). Overlying these are further Holocene age deposits (MIP 1). Assemblage AH I, from the three sections outlined in this study, are Holocene (MIP 1) in age and rest on top of the undated sand-rich aeolian unit within the shelter sequence beneath. The onset of the Holocene is marked by increase rainfall, as evidenced by regional lake records (Parker et al. 2004, 2006, 2016; Preston et al. 2015) and the speleothem record at Hoti Cave (Fleitmann et al. 2011).

Conclusions

New chronometric data revealed that the stratigraphically youngest Middle Palaeolithic layer at Jebel Faya (AH II) represents human occupation of the site at the end of the MIS 5 humid period, about 80 ka ago. Characteristics of the stone artifact assemblage from AH II indicate a preference for elongated flakes with parallel edges, predominately produced by the bidirectional methods. Contemporaneous assemblages from Arabia are rare but those available show important differences, including preferences for ovoid and triangular morphologies produced by centripetal and bidirectional convergent Levallois methods. Based on the chronological data from the bottom (210 ka) and the top of the Palaeolithic sequence (80 ka), we conclude that site FAY-NE1 at Jebel Faya contains an archive of human settlement in the region comprising MIS 7, MIS 6 and MIS 5. Re-occupation of the site occurred after a significant gap during the early Holocene at about 10 ka.

Acknowledgements Results presented here built on work by the long-term collaboration between the University of Tübingen, Germany, and Sharjah Archaeology Authority, Emirate of Sharjah, United Arab Emirates. Initiated by Prof. Hans-Peter Uerpmann, Dr. Margarethe and Dr. Sabah Jasim in the mid-1990s, this project laid foundation for new insights into human early prehistory in Arabia by providing important empirical data. We are grateful to be able to continue this project through ongoing support from Tübingen, provided by Prof. Nicholas J. Conard and his team. We are particularly grateful to Alexander Janas who organized the technical aspects of this project. KB received funding from the Deutsche Forschungsgemeinschaft (grants BR 5562/2-1 and BR 5562/6-1) as well as from the Heidelberg Academy of Sciences

and Humanities through the project "The Role of Culture in Early Expansions of Humans" (ROCEEH). SK would like to thank the French Government for receiving funding through the France Excellence program implemented by the Embassy of France in Korea. KR would like to thank the Faculty of Humanities and Social Sciences, Oxford Brookes University, for postgraduate funding.

Author Contribution K.B., F.P., S.J., E.Y., and A.P. contributed to the study conception and design. K.B., F.P., K.R., G.P., S.K., A.P. performed material preparation, data collection and analysis. K.B., F.P., S.K. and A.P. wrote the manuscript text. All authors reviewed the manuscript.

Funding Open Access funding enabled and organized by Projekt DEAL. This work was supported by Deutsche Forschungsgemeinschaft (Grants BR 5562/2–1 and BR 5562/6–1).

Data Availability Data is provided within the manuscript.

Declarations

Competing interests The authors declare no competing interests. The data that support the findings of this study are published here.

References

Al Farraj A, Harvey AM (2004) Late Quaternary interactions between aeolian and fluvial processes: a case study in the northern UAE. J Arid Environ 56:235–248

Armitage SJ, Jasim SA, Marks AE, Parker AG, Usik VI, Uerpmann H-P (2011) The southern route "out of Africa": evidence for an early expansion of modern humans into Arabia. Science 331:453–456

Atkinson OA, Thomas DS, Parker AG, Goudie AS (2013) Late quaternary humidity and aridity dynamics in the northeast Rub'al-Khali, United Arab Emirates: implications for early human dispersal and occupation of eastern Arabia. Quatern Int 300:292–301

Blinkhorn J, Groucutt HS, Scerri EML, Petraglia MD, Blockley S (2021) Directional changes in Levallois core technologies between Eastern Africa, Arabia, and the Levant during MIS 5. Sci Rep 11:11465

Bretzke K, Herkert K (2023) Jebel Faya and the Middle to Late Pleistocene transition: settlement continuity and behavioral flexibility. Paleorient 49:63–81

Bretzke K, Armitage SJ, Parker AG, Walkington H, Uerpmann H-P (2013) The environmental context of Paleolithic settlement at FAY-NE1, Sharjah Emirate, UAE. Quatern Int 300:83–93

Bretzke K, Conard NJ, Uerpmann H-P (2014) Excavations at Jebel Faya — The FAY-NE1 shelter sequence. In: Proceedings of the Seminar for Arabian Studies 44:69–82

Bretzke K, Preusser F, Jasim SA, Miller C, Preston G, Raith K, Underdown SJ, Parton A, Parker AG (2022) Multiple phases of human dispersal into Arabia between 210,000 and 120,000 years ago. Sci Rep 12:1600

Clemens S, Prell W, Murray D, Shimmield G, Weedon G (1991) Forcing mechanisms of the Indian Ocean monsoon. Nature 353(6346):720–725

Crassard R, Hilbert YH (2013) A Nubian complex site from Central Arabia: implications for Levallois taxonomy and human dispersals during the Upper Pleistocene. PLoS ONE 8(7):e69221

Crassard R, Hilbert YH, Preusser F, Wulf G, Schiettecatte J (2019) Middle Palaeolithic occupations in central Saudi Arabia during MIS 5 and MIS 7: new insights on the origins of the peopling of Arabia. Archaeol Anthropol Sci 11:3101–3120

Degering D, Degering A (2020) Change is the only constant - time-dependent dose rates in luminescence dating. Quat Geochronol 58:101074

Delagnes A, Tribolo C, Bertran P, Brenet M, Crassard R, Jaubert J, Khalidi L, Mercier N, Nomade S, Peigné S, Sitzia L, Tournepiche J-F, Al-Halibi M, Al-Mosabi A, Macchiarelli R (2012) Inland human settlement in southern Arabia 55,000 years ago. New evidence from the Wadi Surdud Middle Paleolithic site complex, western Yemen. J Hum Evol 63:452–474

Dietze M, Kreutzer S, Burow C, Fuchs MC, Fischer M, Schmidt C (2016) The abanico plot: visualising chronometric data with individual standard errors. Quat Geochronol 31:12–18

Drake NA, Breeze P, Parker A (2013) Palaeoclimate in the Saharan and Arabian Deserts during the Middle Palaeolithic and the potential for hominin dispersals. Quatern Int 300:48–61

Eppes MC, Keanini R (2017) Mechanical weathering and rock erosion by climate-dependent subcritical cracking. Rev Geophys 55(2):470–508

Eppes MC, Magi B, Scheff J, Warren K, Ching S, Feng T (2020) Warmer, wetter climates accelerate mechanical weathering in field data, independent of stress-loading. Geophysical Research Letters 47(24):2020GL089062

Farrant AR, Arkley SLB, Ellison RA, Styles MT, Phillips ER (2006) Geology of the Al Dhaid, United Arab Emirates. British geological survey and Ministry of Energy, United Arab Emirates. BGS, Keyworth

Farrant AR, Ellison RA, Thomas RJ, Pharaoh TC, Newell AJ, Goodenough KM, Lee JR, Knox RO (2012) The geology and geophysics of the United Arab Emirates. Volume 6: geology of the western and central United Arab Emirates. British Geological Survey and Ministry of Energy, United Arab Emirates. BGS, Keyworth

Farrant AR, Duller GA, Parker AG, Roberts HM, Parton A, Knox RW, Bide T (2015) Developing a framework of Quaternary dune accumulation in the northern Rub' al-Khali, Arabia. Quatern Int 382:132–144

Fleitmann D, Burns SJ, Neff U, Mangini A, Matter A (2003) Changing moisture sources over the last 330,000 years in northern Oman from fluid-inclusion evidence in speleothems. Quatern Res 60:223–232

Fleitmann D, Burns SJ, Pekala M, Mangini A, Al-Subbary A, Al Aowah M, Kramers J, Matter A (2011) Holocene and Pleistocene pluvial periods in Yemen, southern Arabia. Quatern Sci Rev 30:783–787

Folk RL, Ward WC (1957) Brazos River bar: A study in the significance of grain size parameters. J Sediment Petrol 27:3–26

Fookes PG, Hawkins AB (1988) Limestone weathering: its engineering significance and a proposed classification scheme. Q J Eng GeolHydrogeol 21(1):7–31

Galbraith RF, Roberts RG (2012) Statistical aspects of equivalent dose and error calculation and display in OSL dating: an overview and some recommendations. Quat Geochronol 11:1–27

Groucutt HS, White TS, Clark-Balzan L, Parton A, Crassard R, Shipton C, Jennings RP, Parker AG, Breeze PS, Scerri EML, Alsharekh A, Petraglia MD (2015) Human occupation of the Arabian Empty Quarter during MIS5: evidence from Mundafan Al-Buhayrah, Saudi Arabia. Quat Sci Rev 119:116–135

Groucutt HS, Breeze P, Drake NA, Jennings R, Parton A, White T, Shipton C, Clark-Balzan L, Al-Omari A, Cuthbertson P, Wedage OMC, Bernal MA, Alsharekh A, Petraglia MD (2016) The Middle Palaeolithic of the Nejd, Saudi Arabia. J Field Archaeol 1–17

Groucutt HS, Grün R, Zalmout IAS, Drake NA, Armitage SJ, Candy I, Clark-Wilson R, Louys J, Breeze PS, Duval M, Buck LT, Kivell TL, Pomeroy E, Stephens NB, Stock JT, Stewart M, Price GJ, Kinsley L, Sung WW, Alsharekh A, Al-Omari A, Zahir M, Memesh AM, Abdulshakoor AJ, Al-Masari AM, Bahameem AA, Al Murayyi KMS, Zahrani B, Scerri ELM, Petraglia MD (2018) Homo sapiens in Arabia by 85,000 years ago. Nat Ecol Evol 2:800–809

Groucutt HS, Scerri EML, Stringer C, Petraglia MD (2019) Skhul lithic technology and the dispersal of Homo sapiens into Southwest Asia. Quatern Int 515:30–52

Groucutt HS, White TS, Scerri EML, Andrieux E, Clark-Wilson R, Breeze PS, Armitage SJ, Stewart M, Drake N, Louys J, Price GJ, Duval M, Parton A, Candy I, Carleton WC, Shipton C, Jennings RP, Zahir M, Blinkhorn J, Blockley S, Al-Omari A, Alsharekh AM, Petraglia MD (2021) Multiple hominin dispersals into Southwest Asia over the past 400,000 years. Nature 595:376–380

Heiri O, Lotter AF, Lemcke G (2001) Loss on ignition as a method for estimating organic and carbonate content in sediments: reproducibility and comparability of results. J Paleolimnol 25:101–110

Hovers E (1992) The Lithic Assemblages of Qafzeh Cave. Oxford University Press, Oxford

Jennings RP, Parton A, Clark-Balzan L, White TS, Groucutt HS, Breeze PS, Parker AG, Drake NA, Petraglia MD (2016) Human occupation of the northern Arabian interior during early Marine Isotope Stage 3. J Quat Sci 31:e2920

Krbetschek MR, Rieser U, Zöller L, Heinicke L (1994) Radioactive disequilibria in palaeodosimetric dating of sediments. Radiat Meas 23:485–489

Leuschner DC, Sirocko F (2003) Orbital insolation forcing of the Indian Monsoon–a motor for global climate changes? Palaeogeogr Palaeoclimatol Palaeoecol 197(1–2):83–95

Mueller D, Raith K, Bretzke K, Fülling A, Parker AG, Parton A, Preston GW, Jasim S, Yousif E, Preusser F (2023) Luminescence chronology of fluvial and aeolian deposits from the Emirate of Sharjah, UAE. Quatern Res 112:111–127

Murray AS, Wintle AG (2000) Luminescence dating of quartz using an improved single-aliquot regenerative-dose protocol. Radiat Meas 32:57–73

Olley JM, Murray A, Richard RG (1996) The effects of disequilibria in the uranium and thorium decay chains on burial dose rates in fluvial sediments. Quatern Sci Rev 15:751–760

Parker AG (2009) Pleistocene climate change in Arabia: developing a framework for hominin dispersal over the last 350 ka. In: Petraglia MD, Rose JI (eds) The Evolution of Human Populations in Arabia, Vertebrate Paleobiology and Paleoanthropology. Springer, Dordrecht, pp 39–49

Parker AG, Eckersley L, Smith MM, Goudie AS, Stokes S, White K, Hodson MJ (2004) Holocene vegetation dynamics in the northeastern Rub' al-Khali desert, Arabian Peninsula: a pollen, phytolith and carbon isotope study. J Quat Sci 19:665–676

Parker AG, Goudie AS, Stokes S, White K, Hodson MJ, Manning M, Kennet D (2006) A record of Holocene climate change from lake geochemical analyses in southeastern Arabia. Quatern Res 66:465–476

Parker AG, Preston GW, Parton A, Walkington H, Jardine PE, Leng MJ, Hodson MJ (2016) Low latitude Holocene hydroclimate derived from lake sediment flux and geochemistry. J Quat Sci 31:286–299

Parton A, Farrant AR, Leng MJ, Telfer MW, Groucutt HS, Petraglia MD, Parker AG (2015) Alluvial fan records from southeast Arabia reveal multiple windows for human dispersal. Geology 43:295–298

Parton A, White TS, Parker AG, Breeze PS, Jennings R, Groucutt HS, Petraglia MD (2015) Orbital-scale climate variability in Arabia as a potential motor for human dispersals. Quatern Int 382:82–97

Petraglia MD, Alsharekh A, Breeze P, Clarkson C, Crassard R, Drake NA, Groucutt HS, Jennings R, Parker AG, Parton A, Roberts RG, Shipton C, Matheson C, al-Omari A, Veall M-A (2012) Hominin dispersal into the nefud desert and middle palaeolithic settlement along the Jubbah Palaeolake, Northern Arabia. PLOS ONE 7:e49840

Pourmand A, Marcantonio F, Schulz H (2004) Variations in productivity and eolian fluxes in the northeastern Arabian Sea during the past 110 ka. Earth Planet Sci Lett 221(1–4):39–54

Prescott JR, Hutton JT (1994) Cosmic ray contributions to dose rates for luminescence and ESR dating: large depths and long-term time variations. Radiat Meas 23:497–500

Preston GW, Thomas DSG, Goudie AS, Atkinson O, Leng MJ, Hodson MJ, Walkington H, Charpentier V, Mery S, Borgi F, Parker AG (2015) A multi-proxy analysis of the Holocene humid phase from the United Arab Emirates and its implications for southeast Arabia's Neolithic populations. Quatern Int 382:277–292

Preusser F, Degering D, Fülling A, Miocic JM (2023) Complex dose rate calculations in luminescence dating of lacustrine and palustrine sediments from Niederweningen, northern Switzerland. Geochronometria 50:28–49

Prévost M, Zaidner Y (2020) New insights into early MIS 5 lithic technological behavior in the Levant: Nesher Ramla, Israel as a case study. PLoS ONE 15:e0231109

Richter D, Richter A, Dornich K (2015) Lexsyg smart — a luminescence detection system for dosimetry, material research and dating application. Geochronometria 42:202–209

Rose JI (2010) New light on human prehistory in the Arabo-Persian Gulf Oasis. Curr Anthropol 51:849–883

Rose JI, Usik VI, Marks AE, Hilbert YH, Galletti CS, Parton A, Geiling JM, Černý V, Morley MW, Roberts RG (2011) The Nubian Complex of Dhofar, Oman: an African Middle Stone Age industry in southern Arabia. PLoS ONE 6:e28239

Rose JI, Hilbert YH, Marks AE, Usik VI (2019) The First Peoples of Oman - Paleolithic Archaeology of the Nejd Plateau. Archaeopress, Oxford

Russell N (2014) Optically stimulated luminescence dating of archaeological and environmental sequences in North Africa and Arabia (Doctoral dissertation, Royal Holloway, University of London)

Scerri EML, Groucutt HS, Jennings RP, Petraglia MD (2014) Unexpected technological heterogeneity in northern Arabia indicates complex Late Pleistocene demography at the gateway to Asia. J Hum Evol 75:125–142

Schulz H, von Rad U, Erlenkeuser H, von Rad U (1998) Correlation between Arabian Sea and Greenland climate oscillations of the past 110,000 years. Nature 393(6680):54–57

Shea JJ (2013) Stone tools in the Paleolithic and Neolithic Near East: a guide. Cambridge University Press, New York

Uerpmann HP, Uerpmann M, Kutterer A, Jasim SA (2013) The Neolithic period in the Central Region of the Emirate of Sharjah (UAE). Arab Archaeol Epigr 24(1):102–108

Usik V, Rose JI, Hilbert YH, Van Peer P, Marks AE (2013) Nubian Complex reduction strategies in Dhofar, Southern Oman. Quatern Int 300:244–266

White WB (2007) Cave sediments and paleoclimate. J Cave Karst Studies 69:76–93

Wintle AG, Murray AS (2006) A review of quartz optically stimulated luminescence characteristics and their relevance in single-aliquot regeneration dating protocols. Radiat Meas 41:369–391